



**HAL**  
open science

## Why is mechanical fatigue different from toughness in elastomers? The role of damage by polymer chain scission

Gabriel E. Sanoja, Xavier P. Morelle, Jean Comtet, C. Joshua Yeh, Matteo Ciccotti, Costantino Creton

### ► To cite this version:

Gabriel E. Sanoja, Xavier P. Morelle, Jean Comtet, C. Joshua Yeh, Matteo Ciccotti, et al.. Why is mechanical fatigue different from toughness in elastomers? The role of damage by polymer chain scission. *Science Advances*, 2021, 10.1126/sciadv.abg9410. hal-03871381v2

**HAL Id: hal-03871381**

**<https://hal.science/hal-03871381v2>**

Submitted on 25 Nov 2022

**HAL** is a multi-disciplinary open access archive for the deposit and dissemination of scientific research documents, whether they are published or not. The documents may come from teaching and research institutions in France or abroad, or from public or private research centers.

L'archive ouverte pluridisciplinaire **HAL**, est destinée au dépôt et à la diffusion de documents scientifiques de niveau recherche, publiés ou non, émanant des établissements d'enseignement et de recherche français ou étrangers, des laboratoires publics ou privés.

## APPLIED SCIENCES AND ENGINEERING

# Why is mechanical fatigue different from toughness in elastomers? The role of damage by polymer chain scission

Gabriel E. Sanoja<sup>1,2\*</sup>, Xavier P. Morelle<sup>1†</sup>, Jean Comtet<sup>1</sup>, C. Joshua Yeh<sup>1‡</sup>, Matteo Ciccotti<sup>1</sup>, Costantino Creton<sup>1,3\*</sup>

Although elastomers often experience 10 to 100 million cycles before failure, there is now a limited understanding of their resistance to fatigue crack propagation. We tagged soft and tough double-network elastomers with mechanofluorescent probes and quantified damage by sacrificial bond scission after crack propagation under cyclic and monotonic loading. Damage along fracture surfaces and its spatial localization depend on the elastomer design, as well as on the applied load (i.e., cyclic or monotonic). The key result is that reversible elasticity and strain hardening at low and intermediate strains dictates fatigue resistance, whereas energy dissipation at high strains controls toughness. This information serves to engineer fatigue-resistant elastomers, understand fracture mechanisms, and reduce the environmental footprint of the polymer industry.

## INTRODUCTION

Elastomers are ubiquitous in engineering applications that require large reversible deformations such as tyres, belts, dampers, and seals (1). Although toughness remains an important design consideration to prevent catastrophic failure at high loads, mechanical lifetime is often controlled by the progressive growth of an inherent flaw over numerous cycles of low load. This mechanical degradation is evaluated with durability tests based on fatigue crack propagation, where the crack growth rate of a precracked specimen is monitored over a range of cyclic deformations (or energy release rates) (2, 3). Typically, elastomers suffer from fatigue crack propagation at low cyclic loads and exhibit cyclic fatigue thresholds  $G_0 \sim 0.05$  to  $0.1 \text{ kJ m}^{-2}$  (at which the crack is effectively stopped) substantially below the fracture toughness  $G_c \sim 1$  to  $100 \text{ kJ m}^{-2}$  (as measured by crack propagation under monotonic loading) (4, 5). A fundamental understanding of this fracture behavior would serve to mitigate overengineering, extend lifetime, and facilitate the transition toward a more sustainable elastomer economy.

Fatigue crack propagation has been previously investigated in elastomers (3, 6–8) and, more recently, in hydrogels (9–12). A comparison of the fracture behavior of these materials under monotonic and cyclic loading illustrates some vexing features of fatigue crack propagation. Under monotonic loading, precracked specimens of hydrogels based on ionically cross-linked alginate interpenetrated with covalently cross-linked polyacrylamide exhibit a fracture toughness  $G_c \sim 10 \text{ kJ m}^{-2}$  similar to that of filled elastomers (13). However, under cyclic loading, these hydrogels have a crack growth rate  $dc/dN \sim 100 \text{ nm cycle}^{-1}$  significantly higher than that of filled

elastomers  $dc/dN \sim 1 \text{ nm cycle}^{-1}$  at the same applied energy release rate  $G \sim 0.1 \text{ kJ m}^{-2}$  (7, 10). These observations indicate not only that filled elastomers have a longer mechanical lifetime than hydrogels but also that the mechanisms responsible for reinforcement change when transitioning from monotonic to cyclic loading. This is the reason why energy dissipation by irreversible damage during the first cycle of deformation (i.e., so-called Mullins effect) is not necessarily correlated with fatigue resistance (11, 12). As the subsequent cycles are usually at high frequency and low load, it is the evolution of the crack tip with sustained opening and closing that is presumably key for fatigue crack propagation.

Here, we use soft and tough double-network (DN) elastomers as model materials to investigate fatigue crack propagation. These are composed of a prestretched, stiff, and continuous filler network embedded in a highly extensible, soft, and incompressible matrix network. Although their elastic properties are mainly controlled by the filler network, as in conventional filled elastomers, their fracture toughness primarily results from energy dissipation by sacrificial bond scission during stress transfer to the matrix network (14, 15). This toughening mechanism was recently demonstrated by tagging the filler network with mechanoluminescent damage-activated probes (i.e., mechanophores), monotonically loading a precracked specimen, and visualizing sacrificial bond scission ahead of the crack tip in a time-resolved manner (16). However, under cyclic loading a similar precracked specimen suffers negligible scission of sacrificial bonds per cycle, making visualization of cumulative damage by sacrificial bond scission more valuable to understand fatigue crack propagation. Thus, we tagged the filler network of DN elastomers with mechanofluorescent probes based on  $\pi$ -extended anthracene-maleimide adducts. Upon polymer chain elongation until failure, these probes undergo a force-induced cycloreversion reaction that results in  $\pi$ -extended anthracene moieties (i.e., fluorophores) of high quantum yield, stability to photobleaching (17, 18), and ideal for visualizing and quantifying damage by sacrificial bond scission near the crack surface of fractured specimens (19). This combination of network design and damage quantification is what ultimately provides unprecedented insights on the difference between mechanical durability and fracture toughness in elastomers.

<sup>1</sup>Sciences et Ingénierie de la Matière Molle, ESPCI Paris, Université PSL, Sorbonne Université, CNRS UMR 7615, 75005 Paris, France. <sup>2</sup>McKetta Department of Chemical Engineering, The University of Texas at Austin, Austin, TX, 78712, USA. <sup>3</sup>Global Station for Soft Matter, Global Institution for Collaborative Research and Education, Hokkaido University, 001-0021 Sapporo, Japan.

\*Corresponding author. Email: gesanoja@che.utexas.edu (G.E.S.); costantino.creton@espci.psl.eu (C.C.)

†Present address: Ingénierie des Matériaux Polymères, Université Claude Bernard Lyon 1, INSA de Lyon, Université Jean Monnet de St Etienne, CNRS UMR 5233, 69622 Villeurbanne, France.

‡Present address: 3M Research Center, Saint Paul, MN 55144, USA.

## RESULTS AND DISCUSSION

We synthesized two DN elastomers through sequential free radical polymerization of ethyl acrylate (EA). Detailed synthetic conditions, compositions, and mechanical properties are provided in Materials and Methods and the Supplementary Materials (fig. S1 and tables S1 to S3), but their primary difference lies in the cross-linking density of the filler network, which is 0.2 mole percent (mol %) for EA<sub>0.2</sub>EA and 0.5 mol % for EA<sub>0.5</sub>EA (Fig. 1A). Thus, EA<sub>0.2</sub>EA is tougher and more extensible than EA<sub>0.5</sub>EA (see onset of strain hardening and strain at break in Fig. 1B) even if both elastomers have the same monomer composition, prestretch of the filler network, Young's modulus (Table 1 and Fig. 1, inset), and negligible mechanical hysteresis under step cyclic loading until fracture (fig. S3). Note that as previously reported by Ducrot *et al.* (16), these DN elastomers do not dissipate energy during the first cycle of deformation because of their moderate prestretch  $\lambda_0 \approx 1.7$ , relative to that of other Mullins-like soft materials like triple-network elastomers ( $\lambda_0 \approx 2.5$ ) (14) and osmotically swollen DN hydrogels ( $\lambda_0 \approx 4.6$ ) (11, 20, 21). However, this elastic behavior (i.e., lack of mechanical hysteresis) under uniaxial deformation is misleading because energy dissipation by sacrificial bond scission is actually important for toughening and localized in a large strain region ahead of the crack tip referred to as damage zone (16).

Differences in mechanical properties between the two DN elastomers are subtle but important for rationally engineering fatigue-resistant elastomers. As outlined by Suo and co-workers in their seminal investigations on hydrogels, energy dissipation by sacrificial bond scission leads to toughening in monotonic loading, but accumulation of these scission events ahead of the crack tip could favor crack growth and decrease fatigue resistance (11, 12). Given that EA<sub>0.2</sub>EA and EA<sub>0.5</sub>EA exhibit near-perfect elasticity until failure, we deemed them good model materials to (i) investigate the role of cross-linking density of the filler network on fatigue crack propagation and (ii) build a multiscale picture of fracture under cyclic and monotonic loading using mechanofluorescent probes to reconstruct three-dimensional (3D) maps of cumulative damage by sacrificial bond scission.

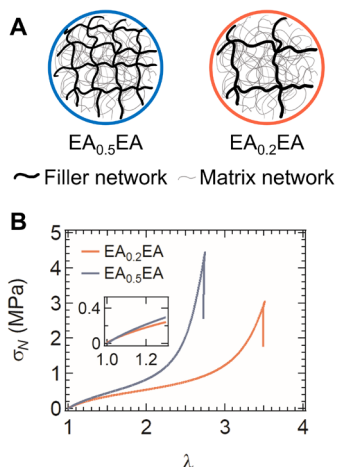


**Fig. 1. Uniaxial deformation of DN elastomers.** (A) Schematic of DN elastomers indicating differences in cross-linking density of the filler network. (B) EA<sub>0.2</sub>EA and EA<sub>0.5</sub>EA have a similar modulus (inset) but a different onset of strain hardening and strain at break.

## Trade-off between durability and toughness in DN elastomers

We evaluated the fatigue crack propagation of the two DN elastomers with durability tests similar to those pioneered for vulcanized elastomers (22) and tough hydrogels (12). Precracked pure-shear specimens were subjected to cyclic loading at a frequency of 10 Hz and an applied energy release rate  $G$ , and the evolution of the crack length  $c$  monitored with the applied number of cycles  $N$  (Fig. 2A). These durability tests on specimens of pure-shear geometry lead to an applied energy release rate  $G$  independent of crack length  $c$  (22, 23), enabling optimum use of mechanofluorescent probes by applying a range of energy release rates  $G$  to the same tagged specimen in a successive and stepwise fashion (see detailed estimates of  $G$  from  $\lambda$  in the Supplementary Materials, pure-shear loading curves in fig. S4, and loading conditions in table S5). Results are presented in Fig. 2B (and fig. S5A) and indicate that the crack length  $c$  grows discontinuously (i.e., nonsteadily) with the applied number of cycles  $N$ , meaning that there is a distribution of crack growth rates  $dc/dN$  for each applied  $G$  (see example for  $\lambda = 1.47$  in Fig. 2B, inset). Average crack growth rates  $dc/dN$  and 95% confidence intervals are summarized in Fig. 2C and reveal a power-law (i.e., Paris' law) behavior  $dc/dN \sim G^{3.4}$  for DN elastomers like that of natural rubber (4), SBR (5), and DN hydrogels (11). Figure 2C also illustrates that two crack growth regimes, referred to as fast and slow due to their distinct  $dc/dN$ , coexist near the onset of catastrophic failure (see filled and empty squares in Fig. 2C and videos of fatigue fracture tests in movies S1 and S2). These are observed at  $G \approx G_c$  for EA<sub>0.5</sub>EA but at  $G < G_c$  for EA<sub>0.2</sub>EA (compare dashed lines at  $G_c$  with empty squares at  $G$  at break in Fig. 2C), indicating that subtle changes in the cross-linking density of the filler network have major consequences in the fatigue crack propagation of DN elastomers. EA<sub>0.5</sub>EA is more fatigue resistant than EA<sub>0.2</sub>EA because it exhibits a lower crack growth rate  $dc/dN$  at the same applied energy release rate  $G$ , but it is also more brittle because it undergoes catastrophic crack propagation under monotonic loading at a lower critical energy release rate  $G_c$ . This trade-off between durability and toughness when stiffening the filler network is remarkable when compared to previous reports by Suo and co-workers on DN hydrogels with bulk energy dissipation, where stiffening the matrix network results in both a lower fatigue threshold and fracture toughness (11, 12). The difference might result from entanglements and friction between the polymer chains upon deformation, which are more important in DN elastomers than in DN hydrogels even if both materials are composed of a filler network that acts as a topological constraint to the matrix network (24). Thus, both the filler and matrix networks play a role on fracture under monotonic and cyclic loading, but this is challenging to understand solely by bulk mechanical testing, particularly in DN elastomers without hysteresis under step cyclic loading until failure.

Figure 2C can also be used to estimate the cyclic fatigue threshold  $G_0$  from the energy release rate  $G$  at which the crack does not grow. Although the cyclic fatigue threshold  $G_0$  is theoretically well defined, experimentally, there is always a concern about the number of cycles used to detect crack growth. Here, we had a spatial resolution of  $250 \mu\text{m pixel}^{-1}$  while monitoring the crack length  $c$ , meaning that the minimum crack growth rate  $dc/dN$  that we could measure over a basis of 400,000 cycles is of order  $1 \text{ nm cycle}^{-1}$ . This threshold condition is more rigorous (and time consuming) than the  $100 \text{ nm cycle}^{-1}$  used for tough hydrogels (10, 11), but still one order of magnitude

**Table 1. Composition and mechanical properties of DN elastomers.** The volume fraction  $\phi^{\text{FN}}$ , prestretch  $\lambda_0$ , and maximum extensibility  $\lambda_m^{\text{FN}}$  of the filler network, as well as the Young's modulus  $E$ , strain at break  $\lambda_{\text{break}}$ , toughness  $G_c$ , and areal density of sacrificial polymer chains  $\Sigma_0$  of the double-networks, are presented.

	$\phi^{\text{FN}}$	$\lambda_0$	$\lambda_m^{\text{FN}}$	$E$ (MPa)	$\lambda_{\text{break}}$	$G_c$ (kJ m <sup>-2</sup> )	$\Sigma_0$ (chains m <sup>-2</sup> )
EA <sub>0.2</sub> EA	0.19	1.74	6.70	0.98	3.51	2.70	$4.8 \times 10^{16}$
EA <sub>0.5</sub> EA	0.22	1.67	4.89	1.05	2.74	1.97	$7.2 \times 10^{16}$

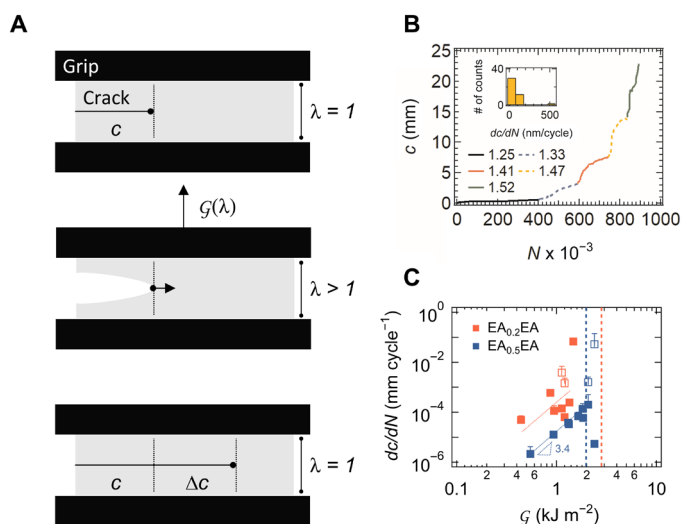


**Fig. 2. Fatigue crack propagation of DN elastomers.** (A) Schematic of a pure shear fatigue fracture test. The pure shear geometry is ideal for studying fracture because the applied energy release rate  $G(\lambda)$  is independent of crack length  $c$  (22, 23). (B) Crack growth of EA<sub>0.5</sub>EA is discontinuous and dependent on the applied stretch  $\lambda$  and energy release rate  $G(\lambda)$ . Inset: Representative distribution of crack growth rates  $dc/dN$  for  $\lambda = 1.47$  or  $G(\lambda) = 1642 \text{ J m}^{-2}$ . A similar fracture behavior is observed for EA<sub>0.2</sub>EA (fig. S5). (C) Fatigue crack propagation of EA<sub>0.2</sub>EA and EA<sub>0.5</sub>EA. EA<sub>0.5</sub>EA is more fatigue resistant than EA<sub>0.2</sub>EA despite its lower toughness  $G_c$  (dashed vertical lines). Open ( $\square$ ) and closed ( $\blacksquare$ ) symbols, respectively, correspond to fast and slow crack growth regimes at the same applied energy release rate  $G(\lambda)$ . Error bars represent 95% confidence intervals.

below the  $0.1 \text{ nm cycle}^{-1}$  used for commercial metallic alloys (25). As EA<sub>0.2</sub>EA exhibits crack growth rates  $dc/dN \sim 10 \text{ nm cycle}^{-1}$  even at low  $G \sim 441 \text{ J m}^{-2}$ , we only determined the cyclic fatigue threshold  $G_0 \sim 550 \text{ J m}^{-2}$  of EA<sub>0.5</sub>EA. This  $G_0$  is similar to that of composite elastomers based on a hard elastomeric lattice embedded in a soft matrix (8) and is remarkable when compared to that of conventional elastomers  $G_0 \sim 50 \text{ J m}^{-2}$  (26–28) and single-network EA<sub>0.5</sub> (we did not measure  $G_0$  for single-network EA<sub>0.5</sub>, but we expect it to be below its fracture toughness  $G_c \sim 150 \text{ J m}^{-2}$ ). Thus, sacrificial bonds provide elastomers with both improved cyclic fatigue thresholds and fracture toughness. This reinforcement under both cyclic and monotonic loading is analogous to that reported by Suo and co-workers on tough hydrogels (10, 11, 13, 20) and intrinsic to the DN architecture. However, the reinforcement mechanism is different. While energy dissipation by sacrificial bond scission is essential for toughening, its role on fatigue resistance remains unclear. A previous model on fatigue crack propagation in glassy polymers, where toughening results from damage by plastic flow

(i.e., crazing), suggests that formation of a crazed region ahead of the crack tip favors crack growth under cyclic loading (29). However, it is unclear whether this model also describes rubbery DN elastomers ( $T_g = -15^\circ\text{C}$ ) that develop a damage zone before crack growth. To gain insights into the role of molecular damage on fatigue crack propagation, we reconstructed 3D maps of damage by sacrificial bond scission in the fractured DN elastomers.

### Visualization and quantification of damage by sacrificial bond scission

Postmortem fluorescent maps of the fracture surface enable visualization and quantification of damage accumulated ahead of the crack tip both before and during crack growth (see example of fluorescent image in Fig. 3B). Details of the methodology are provided in Materials and Methods, in the Supplementary Materials, and in a recent contribution from our group (19). The general idea is based on using the fluorescence of a 3D slab to quantify the per-voxel fraction  $\phi_{xyz}$  of  $\pi$ -extended anthracene moieties resulting from a force-induced cycloreversion reaction in the filler network (Fig. 3A). Given that the probability to break a polymer chain diverges near its limiting extensibility, we considered  $\phi_{xyz}$  as representative of the fraction of bond scission events in the filler network [this hypothesis has been verified in previous work (19) and theoretically described by Dubach *et al.* (30)]. Averaging along the crack length  $x$  and specimen thickness  $z$  (see Fig. 3B) results in profiles of sacrificial bond scission as a function of the distance  $y$  away from the crack surface

$$\phi_y = \left( \frac{1}{wt} \right) \int_0^t \int_0^w \phi_{xyz} dx dz \quad (1)$$

where  $w$  is the width (1000  $\mu\text{m}$ ) and  $t$  is the thickness (160  $\mu\text{m}$ ) of the 3D fluorescent slab. Alternatively, integrating  $\phi_{xyz}$  along  $y$  yields spatial maps of local damage per unit area of crack propagation  $\overline{\Sigma_{xz}}$ , a dimensionless number representing the excess number of broken polymer layers in the filler network per unit area of crack growth

$$\overline{\Sigma_{xz}} = 2 \left( \frac{v_x}{\Sigma_0} \right) \int_0^L \phi_{xyz} dy \quad (2)$$

Here,  $v_x$  and  $\Sigma_0$  are the volumetric and areal density of elastic polymer chains, so that the ratio  $\Sigma_0/v_x$  represents the mesh size of the filler network. These properties can be determined from the modulus using a procedure detailed in the Supplementary Materials (tables S2 and S4) and in the work of Millereau *et al.* (14). We estimate the damage  $\overline{\Sigma_{xz}}$  by integrating over a distance  $y$  from the crack surface  $L \approx 300 \mu\text{m}$  at which  $\phi_{xyz} \approx 0$ , so that we quantify most of the fluorescence and mitigate artefacts from optical vignetting. This distance  $L$  is significantly larger than the mesh size of the filler

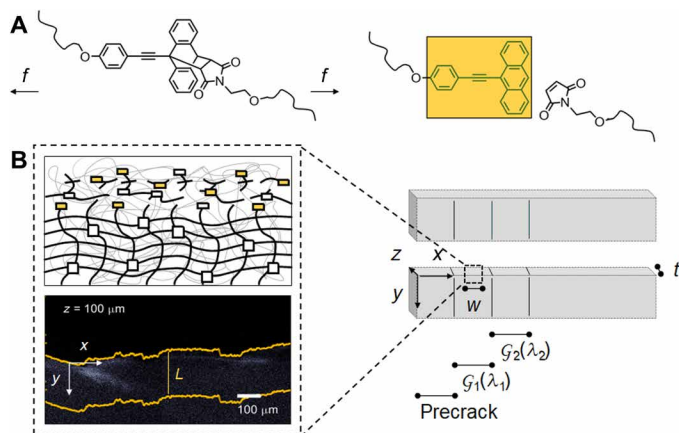


**Fig. 3. Postmortem mapping of damage by sacrificial bond scission.** (A) Mechano-phores based on  $\pi$ -extended anthracene-maleimide adducts yield  $\pi$ -extended anthracene moieties upon force ( $f$ )-induced cycloreversion. (B) Fluorescent microscopy in a fractured specimen reveals high internal damage near the crack surface and around crack bifurcations. Damage by polymer chain scission is quantified over a distance  $L = 300 \mu\text{m}$  from the crack surface. Energy release rates  $G_i(\lambda_i)$  were applied in a subsequent and stepwise fashion to optimize the use of tagged and probe-expensive pure-shear specimens. Photo credit: Gabriel E. Sanoja, ESPCI Paris.

network,  $\Sigma_0/v_x \approx 10 \text{ nm}$ , indicating that damage by sacrificial bond scission extends rather far from the crack surface and into the bulk.

Equation 1 serves to define a dimensionless number representing the average damage per unit area of crack propagation  $\bar{\Sigma}$

$$\bar{\Sigma} = \frac{\Sigma}{\Sigma_0} = 2 \left( \frac{v_x}{\Sigma_0} \right) \int_0^L \phi_y dy \quad (3)$$

where  $\Sigma$  is the average number of broken polymer chains in the filler network per unit area of crack growth. Note that  $\bar{\Sigma}$  is simply the average of  $\Sigma_{xz}$  along the crack length  $x$  and specimen thickness  $z$  and is physically based on the Lake and Thomas molecular theory of fracture of unfilled single-network elastomers (26), where the minimum energy dissipated upon creation of an interface  $\Gamma_0$  is that required to break a monolayer of stretched elastic polymer chains

$$\Gamma_0 = N_x U_b \Sigma_0 \quad (4)$$

Here,  $N_x$  is the number of monomers per elastic polymer chain, and  $U_b$  is the energy stored per C—C bond along the stretched polymer backbone [traditionally, the energy of a C—C bond  $\approx 350 \text{ kJ mol}^{-1}$  but recently revised by Craig and co-workers to  $\approx 60 \text{ kJ mol}^{-1}$  based on a probabilistic view of bond scission (31)]. Hence,  $\bar{\Sigma}$  represents the excess number of broken layers in the filler network per unit area of crack growth and is related to the energy dissipated by covalent bond scission upon fracture  $\Gamma_d$

$$\Gamma_d = \Gamma_0 \bar{\Sigma} = N_x U_b \Sigma_0 \bar{\Sigma} \quad (5)$$

### Effect of cross-linking density of the filler network on the accumulation and localization of damage during fatigue crack propagation of DN elastomers

The visualization and quantification of damage by sacrificial bond scission in fractured specimens is a novel tool to understand the role of the cross-linking density of the filler network on the crack growth

rate of DN elastomers subject to cyclic loading. However, interpreting spatially resolved information on damage is challenging because of the complex relationship between the applied energy release rate  $G$  (or strain  $\lambda$ ) and the resulting crack growth rate  $dc/dN$  and damage per unit area of crack propagation  $\bar{\Sigma}$ .

As illustrated in Fig. 4, the tougher and more extensible  $\text{EA}_{0.2}\text{EA}$  suffers more damage than  $\text{EA}_{0.5}\text{EA}$  when fractured under cyclic loading at the same applied energy release rate  $G \approx 1.0 \text{ kJ m}^{-2}$ . The damage maps in Fig. 4A are rather homogeneous along the crack length  $x$  and specimen thickness  $z$ , with some inhomogeneous artefacts attributed to image stitching and optical vignetting (see details in the Supplementary Materials). This observation is consistent with the featureless side view of the fracture surface (see images for the plane  $z = 100 \mu\text{m}$  in Fig. 4B) and the monotonically decreasing  $y$  profiles of damage from the crack surface  $\phi_y$  (Fig. 4C).  $\text{EA}_{0.2}\text{EA}$  exhibits a considerably higher  $dc/dN$  than  $\text{EA}_{0.5}\text{EA}$  at the same  $G \approx 1.0 \text{ kJ m}^{-2}$  (compare fatigue curves in Fig. 2C), meaning that less cycles  $N$  result in more damage  $\bar{\Sigma}$  for the same unit area of crack growth.

Figure 4 also illustrates changes in damage localization with the cross-linking density of the filler network. Although it is difficult to unambiguously define damage localization, we estimated the thickness of the surface layer over which the DN elastomers are damaged from the distance over which  $\phi_y$  decreases to half its maximum value,  $L_{1/2}$ .  $\text{EA}_{0.5}\text{EA}$  has a larger  $L_{1/2}$  than  $\text{EA}_{0.2}\text{EA}$  (compare  $y$  profiles of  $\phi_y$  in Fig. 4C), indicating that stiffening the filler network results in a more delocalized and gradual decrease of damage ahead of the crack tip during fatigue crack propagation (see schemes of damage zones in Fig. 4D).

Thus, the cross-linking density of the filler network affects both the accumulation  $\bar{\Sigma}$  and localization  $L_{1/2}$  of damage ahead of the crack tip. We attribute this effect to differences in the large strain behavior between the two DN elastomers. Although  $\text{EA}_{0.2}\text{EA}$  and  $\text{EA}_{0.5}\text{EA}$  require somewhat similar bulk strains  $\lambda$  to attain the same applied energy release rate  $G$  (see Table 2), the local strain of  $\text{EA}_{0.2}\text{EA}$  ahead of the crack tip (i.e., inside the damage zone) must be significantly larger than that of  $\text{EA}_{0.5}\text{EA}$  because of its higher extensibility (we did not measure the strain at the crack tip, but can infer the qualitative strain fields of Fig. 4D from images of crack blunting in fig. S10). Large strains ahead of the crack tip, as well as those actually experienced by the filler network relative to its limiting extensibility, increase the probability of damage by sacrificial bond scission, promote stress transfer to the matrix network, and favor crack growth. Hence,  $\text{EA}_{0.2}\text{EA}$  is more damaged than  $\text{EA}_{0.5}\text{EA}$  per loading cycle, meaning that more Lake and Thomas monolayers of polymer chains break in the filler network of the more extensible DN elastomer upon crack growth.

As insightfully noted by a reviewer, this assumption of strain-mediated bond scission and activation of the  $\pi$ -extended anthracene-maleimide adduct is different from that made by Chen *et al.* (32), where the force-mediated ring-opening and activation of spiroiran was used to quantify and map the stress of analogous multiple-network elastomers with  $\lambda_0 \approx 2.5$  and demonstrate that stiffening the filler network increases the stress ahead of the crack tip upon quasi-static loading at the same applied energy release rate  $G$ . In reality, neither assumption is strictly valid because bond scission is strongly influenced by thermal fluctuations, meaning that it is more accurately described as a barrier crossing (i.e., activated) process with an energy landscape biased by an external force (33, 34). Polymer

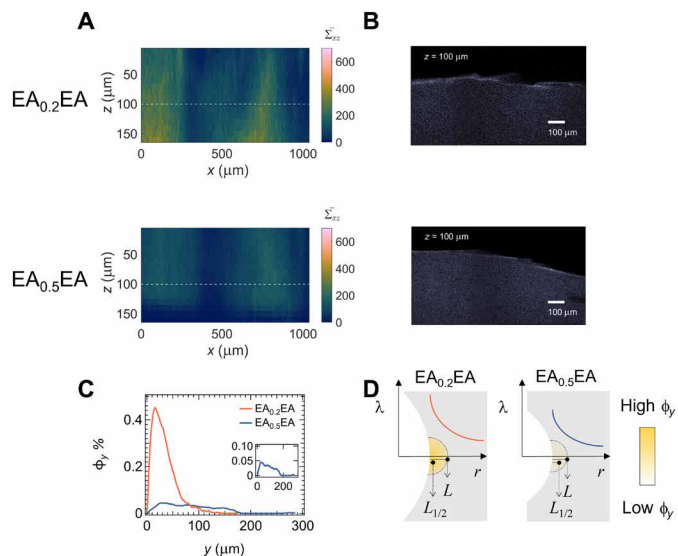


**Fig. 4. Damage of DN elastomers fractured under cyclic loading at  $G \approx 1.0 \text{ kJ m}^{-2}$ .** (A) Spatial maps of local damage per unit area of crack propagation,  $\Sigma_{xz}$ , reveal that EA<sub>0.2</sub>EA is more damaged than EA<sub>0.5</sub>EA. (B) Representative images at  $z = 100 \text{ } \mu\text{m}$  [white dashed line in (A)] illustrate that featureless fracture surfaces are associated with homogeneous damage maps along the crack length. Photo credit: Gabriel E. Sanoja, ESPCI Paris. (C) Profiles of sacrificial bond scission  $\phi_y$  reveal that EA<sub>0.2</sub>EA has a more concentrated and localized damage zone than EA<sub>0.5</sub>EA. Inset: Enlarged profile of sacrificial bond scission  $\phi_y$  of EA<sub>0.5</sub>EA. (D) Schemes of damage zones of DN elastomers undergoing fatigue crack propagation. EA<sub>0.5</sub>EA has reduced (low  $\phi_y$  and  $\Sigma$ ) and delocalized (high  $L_{1/2}$ ) damage ahead of the crack tip and, hence, can sustain many cycles of low deformation before crack growth.

chains experience a range of forces and conformations upon bulk deformation so that their scission is mediated not only by strain and stress but also by temperature and bond dissociation energy. Hence, it is possible that bond scission is primarily mediated by stress when polymer chains are stretched in response to large quasi-static loads, in agreement with Chen *et al.* (32), but by strain amplitude when polymer chains are cycled in response to low cyclic loads and friction may be more important for energy dissipation. This change in molecular mechanism when transitioning from quasi-static to cyclic loading explains why the strain-hardened elastomer, EA<sub>0.5</sub>EA, is less damaged and more fatigue resistant than its tougher counterpart, EA<sub>0.2</sub>EA, even if it is cycled at a higher stress (and lower strain) amplitude. In addition, it highlights that the average damage by sacrificial bond scission  $\Sigma$  does not directly reflect the total amount of energy dissipated upon crack growth or, namely, that the applied energy release rate  $G$  governs the nonlinear stress and stretch fields ahead of the crack tip (i.e., like the stress intensity factor in linear elastic fracture mechanics or the  $J$  integral in nonlinear elastic crack tip solutions) but not the energy dissipated upon crack growth. A more detailed discussion on how to interpret the applied energy release rate  $G$  in the context of fracture of soft materials is provided by Long *et al.* (35). To better understand the role of bond scission on fatigue crack propagation, we systematically quantified the damage of the two DN elastomers across a range of applied energy release rates  $G$ .

### Stable damage zone for durability

Beyond the structure-property relationships of DN elastomers, the visualization and quantification of damage by sacrificial bond scission

**Table 2. Loading conditions and damage properties of DN elastomers fractured under cyclic loading at  $G \approx 1.0 \text{ kJ m}^{-2}$ .** The applied stretch  $\lambda$ , energy release rate  $G$ , crack growth rate  $dc/dN$ , average damage per unit area of crack propagation  $\Sigma$ , and the damage penetration length  $L_{1/2}$  are presented.

	$\lambda$	$G (\text{J m}^{-2})$	$dc/dN \times 10^5$ (mm cycle <sup>-1</sup> )	$\Sigma$	$L_{1/2} (\mu\text{m})$
EA <sub>0.2</sub> EA	1.45	942	11.4	68	75
EA <sub>0.5</sub> EA	1.33	932	1.27	15	127

also serves to build a multiscale picture of fatigue fracture. As illustrated in Fig. 5, the damage per unit area of crack growth  $\Sigma$  increases with the applied energy release rate  $G$  with a power law  $\Sigma \sim G^{2.1}$ . This scaling exponent is lower than that observed for the crack growth rate,  $dc/dN \sim G^{3.4}$  (Fig. 2C), and indicates that damaging DN elastomers results in a more significant increase in  $dc/dN$ . Fracture under cyclic loading at high applied  $G$  requires less cycles  $N$  and results in more damage per unit area of crack growth  $\Sigma$ . Thus, numerous cycles at low deformation are less damaging than few cycles at large deformation or, namely, more energy is dissipated by sacrificial bond scission when transitioning from cyclic to monotonic loading.

Details of the catastrophic failure under cyclic loading are also revealed by inspecting the postmortem damage maps of the two co-existing regimes of crack growth at high applied  $G$  (see filled and empty squares in Figs. 2C and 5). DN elastomers are more damaged in the slow than in the fast crack growth regime (compare fast and slow damage maps of either EA<sub>0.5</sub>EA cycled at  $G \approx 2.1 \text{ kJ m}^{-2}$  in Fig. 6A or of EA<sub>0.2</sub>EA cycled at  $G \approx 1.2 \text{ kJ m}^{-2}$  in fig. S6), having maps with heterogeneities (i.e., hotspots) that indicate damage accumulation at or near crack bifurcations (see representative images for the plane  $z = 100 \text{ } \mu\text{m}$  in Fig. 6B). These damage heterogeneities are sometimes reflected in the  $y$  profiles of  $\phi_y$  but, sometimes, lost in the  $xz$  average (Eq. 1) because of insufficient damage accumulation in the crack bifurcations (compare  $y$  profiles in Fig. 6C). Nonetheless, the  $y$  profiles of  $\phi_y$  can be used to estimate an average  $\Sigma$  and  $L_{1/2}$  and better understand fatigue fracture (Table 3). Accumulation of damage over a large region ahead of many bifurcations (high  $\Sigma$  and  $L_{1/2}$ ) is associated with a low  $dc/dN$ , whereas localization of damage over a small region ahead of few bifurcations (low  $\Sigma$  and  $L_{1/2}$ ) is associated with a high  $dc/dN$  (see schemes of damage zones in Fig. 6D). This interplay between accumulation and localization of damage is also evidenced in the fracture surfaces [see scanning electron microscopy (SEM) images in fig. S11], which exhibit many bifurcation events in both regimes but are rougher when the crack grows slowly. Hence, DN elastomers experience a fluctuating local energy release rate  $G_{\text{local}}$  ahead of the crack tip that depends not only on the bulk strain but also on the mesoscopic bifurcation of the crack front and on the probability of sacrificial bond scission inside the damage zone. A fluctuating  $G_{\text{local}}$  is consistent with the discontinuous crack growth (i.e., slowdown at  $\lambda = 1.41$  in Fig. 2B and speedup at  $\lambda = 1.31$  in fig. S5) and the catastrophic  $dc/dN$  observed at  $G < G_c$  for EA<sub>0.2</sub>EA (Fig. 2C) during fatigue crack propagation.

A multiscale picture of fatigue crack propagation results from damage quantification over a range of applied  $G$  and is based on two stages: formation of a damage zone and crack growth. This

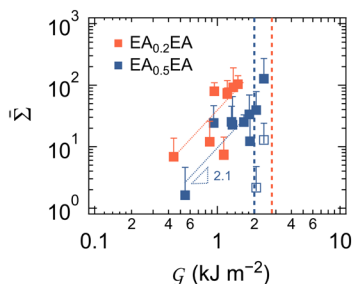


**Fig. 5. Damage of DN elastomers fractured under cyclic loading over a range of  $G$ .** EA<sub>0.2</sub>EA is more damaged than EA<sub>0.5</sub>EA over the entire range of applied energy release rates  $G(\lambda)$ . In addition, both EA<sub>0.2</sub>EA and EA<sub>0.5</sub>EA are more damaged at high energy release rates  $G$ , although less cycles  $N$  are required to attain the same unit area of crack growth. Open ( $\square$ ) and closed ( $\blacksquare$ ) symbols, respectively, correspond to fast and slow crack growth regimes. Dashed vertical lines indicate the fracture toughness  $G_c$ . Error bars represent 95% confidence intervals.

mechanism is similar to that postulated by Williams (29) for glassy polymers like poly(methyl methacrylate), where cyclic loading leads to a plastic zone before fracture. At low applied  $G$ , the stress is primarily sustained by the filler network, there is random scission of sacrificial bonds ahead of the crack tip, and crack growth is controlled by the maximum extensibility of the matrix network. This matrix network is the same for both DN elastomers, and the more strain hardened elastomer, EA<sub>0.5</sub>EA, has the lower probability of crack growth. At high applied  $G$ , an important fraction of the stress is transferred from the filler to the matrix network (32), and sacrificial bond scission can suddenly localize in a zone of reduced  $\bar{\Sigma}$  and localized  $L_{1/2}$  damage that leads to fast crack growth. This transition is similar to that observed by Millereau *et al.* (14) at the yield point of multiple-network elastomers of lower volume fraction of filler network  $\phi^{FN} \approx 0.03$ , where damage by sacrificial bond scission localizes at the fronts of a necked region and is more likely to occur in the elastomer with the lower yield stress, EA<sub>0.2</sub>EA [we could not measure the yield stress of DN elastomers because it is lower than the stress at break, but we know it is lower in EA<sub>0.2</sub>EA from Millereau *et al.* (14) and Chen *et al.* (36)]. Hence, EA<sub>0.5</sub>EA has a more stable damage zone, a lower probability of crack growth, and a better fatigue resistance than EA<sub>0.2</sub>EA.

A more stable damage zone also increases the probability of crack growth through a bifurcated pathway. Upon bifurcation of the crack front, the applied  $G$  decreases to  $G_{local}$  (i.e., the strain field becomes more homogeneous), and damage delocalizes ahead of coexisting crack fronts. This delocalization enables significant damage accumulation before crack growth and leads to more marked differences in  $\bar{\Sigma}$  and  $L_{1/2}$  between the slow and fast crack growth regimes in the more fatigue-resistant elastomer, EA<sub>0.5</sub>EA (Table 3). As a result, damage by sacrificial bond scission and bifurcations of the crack front reinforce each other (i.e., integrate a positive feedback loop) to control the macroscopic crack growth rate  $dc/dN$  of DN elastomers. These mechanisms operate at distinct length scales and depend on the areal density of sacrificial bonds, as well as on the applied load.

Stiffening the filler network strain hardens the region ahead of the crack tip, decreases the probability of sacrificial bond scission, and delocalizes damage over a large region of coexisting bifurcations. This damage zone is more stable to cyclic loading but dissipates less energy by sacrificial bond scission. Hence, fatigue-resistant elastomers capable of sustaining many cycles at low loads are not necessarily

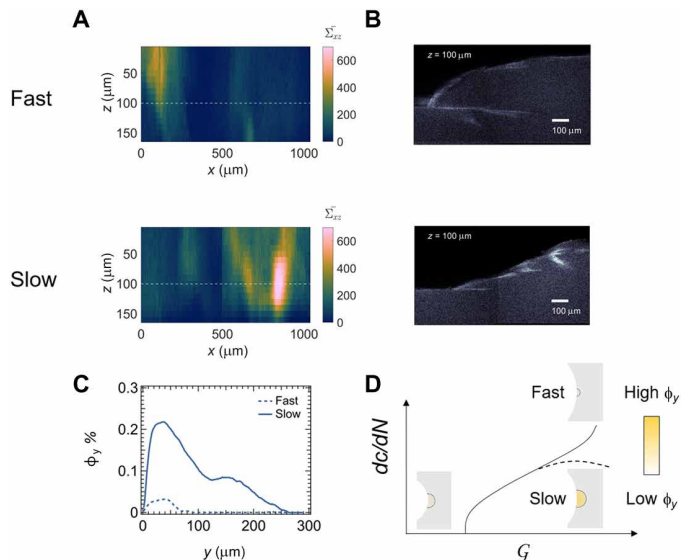


**Fig. 6. Damage of EA<sub>0.5</sub>EA fractured under cyclic loading at  $G \approx 2.1 \text{ kJ m}^{-2}$ .** (A) Spatial maps of local damage per unit area of crack propagation  $\bar{\Sigma}_{xz}$  reveal that EA<sub>0.5</sub>EA is more damaged in the slow than in the fast crack growth regime. (B) Representative images at  $z = 100 \mu\text{m}$  [white dashed line in (A)] illustrate that crack bifurcations are associated with hotspots in damage maps. Photo credit: Gabriel E. Sanoja, ESPCI Paris. (C) Profiles of sacrificial bond scission  $\phi_y$  reveal that EA<sub>0.5</sub>EA undergoes catastrophic crack propagation because of sudden localization of damage ahead of the crack tip. (D) Schematics of the damage zone of EA<sub>0.5</sub>EA in the slow and fast crack growth regimes. Fast crack growth is associated with a highly localized (low  $L_{1/2}$ ) and reduced damage (low  $\phi_y$  and  $\bar{\Sigma}$ ) ahead of the crack tip.

optimum in terms of energy dissipation and toughness. We explored this issue by quantifying damage in DN elastomers fractured under monotonic loading.

### Energy dissipation for toughness

To assess the ability of DN elastomers to dissipate energy, we monitored the crack length  $c$  of a precracked pure-shear specimen subjected to monotonic loading at a fixed stretch rate until fracture (see crack growth curves in fig. 7B and videos of pure-shear fracture tests in movies S3 and S4). As illustrated in Fig. 7B, catastrophic propagation is preceded by a regime of slow crack growth that we refer to as initiation and restrict to  $\Delta c \approx 1 \text{ mm}$ . Under this constraint, the onset of crack initiation is at a stretch  $\lambda_i \approx 1.4$  for EA<sub>0.5</sub>EA and  $\lambda_i \approx 1.7$  for EA<sub>0.2</sub>EA.

Like fracture under cyclic loading, the cross-linking density of the filler network has a significant effect on the accumulation and localization of damage during monotonic fracture. EA<sub>0.5</sub>EA exhibits more heterogeneous damage maps than EA<sub>0.2</sub>EA irrespective of whether the crack grows in the initiation or propagation regime (compare damage maps in Fig. 8A, roughness of fracture surfaces in fig. S12, and fluorescent images for  $z = 100 \mu\text{m}$  in fig. S13), indicating that it is more prone to damage delocalization through bifurcation of the crack front. The  $y$  profiles of  $\phi_y$  also reveal that EA<sub>0.5</sub>EA accumulates  $\bar{\Sigma}$  and delocalizes  $L_{1/2}$  more damage than EA<sub>0.2</sub>EA during crack initiation but not during crack propagation (see Fig. 8, B and C, and Table 4). This change in the damage zone is consistent with the trade-off between fatigue resistance and toughness and in agreement with molecular models that describe the toughness of DN hydrogels

**Table 3. Loading conditions and damage properties of DN elastomers fractured under cyclic loading at high applied energy release rates  $G$ .** The applied stretch  $\lambda$ , energy release rate  $G$ , crack growth rate  $dc/dN$ , average damage per unit area of crack propagation  $\bar{\Sigma}$ , and the damage penetration length  $L_{1/2}$  are presented.

	$\lambda$	$G$ ( $\text{J m}^{-2}$ )	Regime	$dc/dN \times 10^5$ ( $\text{mm cycle}^{-1}$ )	$\bar{\Sigma}$	$L_{1/2}$ ( $\mu\text{m}$ )
<b>EA<sub>0.2</sub>EA</b>	1.49	1205	Fast	144	52	52
			Slow	6.40	81	69
<b>EA<sub>0.5</sub>EA</b>	1.62	2069	Fast	161	5	58
			Slow	20.0	77	100

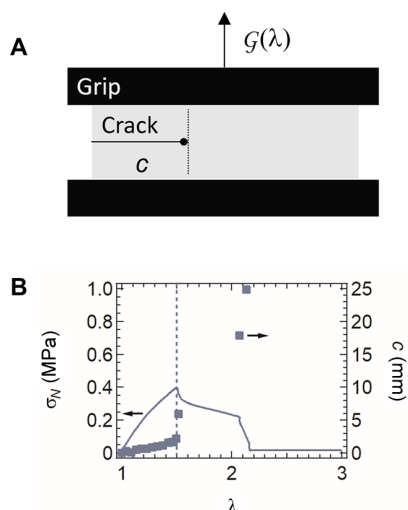


**Fig. 7. Fracture of DN elastomers under monotonic loading.** (A) Schematics of a pure-shear fracture test. (B) Crack growth and loading curve of EA<sub>0.5</sub>EA. The crack growth transitions from the initiation to the propagation regime at the critical stretch  $\lambda_c$  (dashed vertical line).

and glassy polymers (37, 38). DN elastomers capable of accumulating and delocalizing damage at  $G < G_c$  should be more fatigue resistant, whereas those that dissipate more energy at  $G \approx G_c$  should be tougher. The energy dissipated by sacrificial bond scission during monotonic crack propagation,  $\Gamma_b$ , can be estimated from Eq. 5 and is roughly  $\approx 5\%$  of the fracture energy  $G_c$ , suggesting that other molecular processes such as polymer chain friction and stress transfer to the matrix network are important for resisting fracture (i.e., toughening) at high applied energy release rates  $G$  when nonlinear deformations and the damage zone ahead of the crack tip are most prominent. However, these processes likely favor fatigue crack propagation at low applied energy release rates  $G$  when energy dissipation by polymer chain friction might become more significant and the damage zone ahead of the crack tip is controlled by the local strain amplitude.

Quantification of damage by sacrificial bond scission serves to rationally engineer tough and fatigue-resistant elastomers. Under monotonic loading, softening the filler network toughens DN elastomers because more energy is dissipated at the critical energy release rate  $G_c$ , whereas stiffening the filler network improves the fatigue resistance of DN elastomers because the damage zone is more stable to cyclic loading at subcritical energy release rates  $G$ . This is a clear

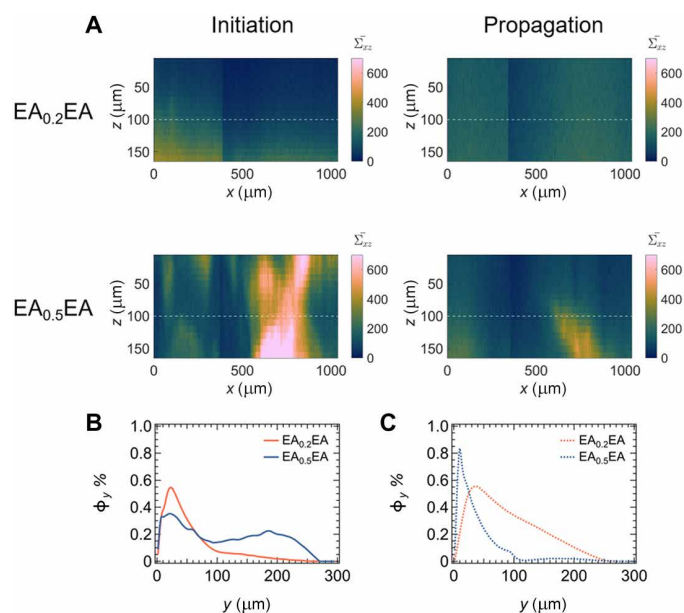


**Fig. 8. Damage of DN elastomers fractured under monotonic loading.** (A) Spatial maps of  $\bar{\Sigma}_{xz}$  reveal that EA<sub>0.5</sub>EA exhibits a more heterogeneous damage than EA<sub>0.2</sub>EA in the initiation and propagation regimes. Profiles of  $\phi_y$  during crack (B) initiation and (C) propagation illustrate that the length scale over which bonds are broken depends on whether the energy supplied during loading is above or below  $G_c$ .

demonstration of the role of network architecture on the damage zone, as well as on the trade-off between mechanical durability and fracture toughness.

### Concluding remarks

Soft and tough DN elastomers tagged with mechanofluorescent probes provide novel insights on fatigue crack propagation. Upon polymer chain elongation until failure, these probes turn into fluorescent moieties of high quantum yield, stability to photobleaching, and ideal for quantifying cumulative damage by sacrificial bond scission in specimens that suffer negligible damage per unit time (i.e., cycle). Hence, this combination of network design and damage quantification has enormous potential to understand fracture of soft materials under a range of complex loading configurations like multiaxial fatigue and cavitation (39).

DN elastomers exhibit a trade-off between fatigue resistance and fracture toughness. While dissipating energy by sacrificial bond scission over large damage zones remains essential for resisting crack

**Table 4. Damage properties of DN elastomers fractured under monotonic loading.** The average damage per unit area of crack propagation  $\Sigma$  and the penetration length  $L_{1/2}$  are presented.

	Regime	$\Sigma$	$L_{1/2}$ ( $\mu\text{m}$ )
EA <sub>0.2</sub> EA	Initiation	72	57
	Propagation	141	129
EA <sub>0.5</sub> EA	Initiation	153	223
	Propagation	95	32

propagation at high loads, stabilizing the damage zone by mitigating the accumulation and localization of sacrificial bond scission events is critical for sustaining numerous cycles of low load. Such stable damage zone is attained in DN elastomers by stiffening the filler network (i.e., strain hardening the region ahead of the crack tip) to reduce the probability of sacrificial bond scission and promote bifurcation of the crack front. Given the similarity in composition, modulus, and bulk hysteresis of EA<sub>0.2</sub>EA and EA<sub>0.5</sub>EA, this inversion in reinforcement when transitioning from monotonic to cyclic loading is remarkable.

DN elastomers exhibit outstanding fatigue thresholds. Cycling the fatigue-resistant elastomer, EA<sub>0.5</sub>EA, for 400,000 cycles at low applied energy release rates  $G \approx G_0 \approx 550 \text{ J m}^{-2}$  leads to negligible crack growth. This cyclic fatigue threshold is substantially higher than that of conventional elastomers and intrinsic to the multiple-network architecture. However, DN elastomers suffer from strain-dependent damage under cyclic loading, developing a zone of accumulated and delocalized damage at high applied energy release rates  $G$  that is prone to sudden localization and fast crack growth. This dependence of damage on the applied load serves as experimental evidence to refine current molecular models of fracture, like that of Lake and Thomas (6), Olsen and co-workers (40), and Zhao and co-workers (41), where the contribution of damage to the fracture energy results only from scission of stretched polymer chains in a damage zone of mesh size.

Last, DN elastomers are nearly elastic (i.e., negligible mechanical hysteresis) at low strains but dissipate energy by sacrificial bond scission above a critical strain. This combination of mechanical properties is characteristic of elastic dissipaters: soft materials composed of a stiff, brittle, and elastic phase embedded in a soft, stretchable, and elastic matrix (42). Thus, DN elastomers behave as molecular composites, as seminally reported by Millereau *et al.* (14). Additional examples of elastic dissipaters include composites of poly(dimethyl siloxane) elastomers (8, 42) and polyacrylamide hydrogels (43). These materials dissipate energy only at high strains to prevent catastrophic failure and delocalize the stress concentration to delay crack growth over numerous cycles of low strain. Other materials, instead, dissipate energy at every strain for toughness and delocalize the strain concentration for fatigue resistance. Examples include semicrystalline poly(vinyl alcohol) hydrogels (44, 45) and strain-crystallizable natural rubber (4). Such fundamental understanding of the mechanical properties serves to develop novel soft, tough, and durable materials for engineering applications (e.g., tyres and dampers), energy conversion and storage devices (e.g., wearable electronics, ion gels), and medicine (e.g., prosthetics). However, we advise caution when drawing analogies between DN elastomers and other soft

materials because subtle differences in molecular structure and stress transfer between soft and stiff domains could change the underlying mechanisms governing mechanical fatigue and fracture toughness.

## MATERIALS AND METHODS

### Materials

EA, 1,4-butanediol diacrylate (BDA) and 2-hydroxy-2-methylpropiophenone (HMP) were purchased from Sigma-Aldrich. EA and BDA were eluted over activated alumina, whereas HMP was used as received. The mechanofluorescent  $\pi$ -extended anthracene maleimide probe, a Diels-Alder cross-linker (DACL), was synthesized and purified according to previously established procedures (17). All reagents were sparged with  $\text{N}_2$  for 45 min and transferred to a  $\text{N}_2$ -filled glovebox.

### Synthesis of SN elastomers EA<sub>x</sub>

Filler networks were synthesized via ultraviolet (UV)-initiated bulk polymerization of EA. In a  $\text{N}_2$ -filled glovebox, monomer EA, co-cross-linkers BDA and DACL, and initiator HMP were well mixed in a scintillation vial and subsequently transferred to a mold composed of two polyethylene terephthalate (PET)-covered glass plates sealed with a silicone spacer ( $\approx 0.1 \text{ mm}$ ). Polymerization was conducted for 2 hours under UV irradiation ( $10 \mu\text{m cm}^{-2}$ ), and the resulting single networks were dried overnight at  $50^\circ\text{C}$  under vacuum. Detailed compositions of the filler networks are summarized in table S1.

### Synthesis of DN elastomers EA<sub>x</sub>EA

In a  $\text{N}_2$ -filled glovebox, filler networks were swollen to equilibrium in a solution of monomer EA (99.98 mol %), cross-linker BDA (0.01 mol %), and initiator HMP (0.01 mol %) and subsequently transferred to a mold composed of two PET-covered glass plates. Polymerization was conducted for 2 hours under UV irradiation ( $10 \mu\text{m cm}^{-2}$ ), and the resulting double networks were dried overnight at  $50^\circ\text{C}$  under vacuum.

### Uniaxial deformation

DN elastomers were punchcut into dog bone-shape specimens of 20 mm in length, 4 mm in width, and  $\approx 1.4 \text{ mm}$  in thickness as defined by the swelling ratio of the filler network. These were marked with two dots of white paint and subsequently deformed at  $1.0 \text{ mm s}^{-1}$  ( $0.05 \text{ s}^{-1}$ ) with an Instron 5965 equipped with a 100-N load cell and a video extensometer.

### Fracture under monotonic loading

DN elastomers were cut into pure shear specimens of  $\approx 30 \text{ mm}$  in length and  $\approx 1.4 \text{ mm}$  in thickness as defined by the swelling ratio of the filler network. These were marked with two dots of white paint and subsequently loaded with crossheads separated by  $\approx 14.5 \text{ mm}$  either on an Instron 5965 or a servohydraulic Zwick/Roell Hamsler HC25 equipped with a 100-N and a 5-kN load cell, respectively. Specimens were deformed at a crosshead speed of  $0.73 \text{ mm s}^{-1}$  ( $0.05 \text{ s}^{-1}$ ) while monitoring the stretch with a video extensometer for EA<sub>0.5</sub>EA and the crosshead displacement for EA<sub>0.2</sub>EA. These experiments were conducted on pristine and precracked specimens ( $\approx 6\text{-mm}$  crack from a fresh razor blade) to determine the applied energy release rate  $G$  as a function of the applied strain  $\lambda$  according to previously established procedures (22). Noteworthy, the pure shear specimens did not slip from the crossheads when subject to low deformations such that the stress-stretch curves under uniaxial

and pure shear deformation overlap below the critical strain for crack propagation  $\lambda_c$ .

### Fracture under cyclic loading

DN elastomers were cut into pure shear specimens of  $\approx 30$  mm in length and  $\approx 1.4$  mm in thickness as defined by the swelling ratio of the filler network. These were notched with a fresh razor blade and subsequently loaded on a servohydraulic Zwick/Roell Hamsler HC25 equipped with a 5-kN load cell and crossheads covered with millimeter paper. Specimens were deformed at a displacement-controlled frequency of 10 Hz while monitoring the crack length with a Baumer camera.

### Visualization of damage by sacrificial bond scission

Fractured specimens were cleaned with ethanol and optical paper, taped to a petri dish with double-sided tape, and immersed in glycerol to mitigate refraction at the crack surface. Fluorescent images were acquired on a customized Nikon AZ-100/C2+ confocal microscope equipped with an AZ Plan Fluor 5 $\times$  objective of 15-mm focal length.  $\pi$ -Extended anthracene fluorophores were excited with a 405-nm laser, and their fluorescent emission was recorded in the range of 424 to 524 nm. The optical magnification was set to  $\times 5$ , resulting in  $512 \times 512$  raw images ( $1.63 \mu\text{m pixel}^{-1}$ ) that were subsequently stitched with a 20% overlap. 3D scans were collected from the specimen surface (i.e., plane of maximum intensity) through a  $160 \mu\text{m}$  depth using a step size of  $10 \mu\text{m}$ .

### Scanning electron microscopy

Fractured specimens were imaged with a Thermo Fisher Scientific SEM Quattro FEI operating under vacuum at a fixed potential of 5.00 kV.

### SUPPLEMENTARY MATERIALS

Supplementary material for this article is available at <https://science.org/doi/10.1126/sciadv.abg9410>

### REFERENCES AND NOTES

- A. N. Gent, *Engineering with Rubber* (Hanser, ed. 3, 2012); [www.sciencedirect.com/science/article/pii/B9783446427648500181](https://www.sciencedirect.com/science/article/pii/B9783446427648500181).
- G. J. Lake, Fatigue and fracture of elastomers. *Rubber Chem. Technol.* **68**, 435–460 (1995).
- W. V. Mars, A. Fatemi, Factors that affect the fatigue life of rubber: A literature survey. *Rubber Chem. Technol.* **77**, 391–412 (2004).
- A. N. Gent, P. B. Lindley, A. G. Thomas, Cut growth and fatigue of rubbers. I. The relationship between cut growth and fatigue. *J. Appl. Polym. Sci.* **8**, 455–466 (1964).
- G. J. Lake, P. B. Lindley, Cut growth and fatigue of rubbers. II. Experiments on a noncrystallizing rubber. *J. Appl. Polym. Sci.* **8**, 707–721 (1964).
- G. J. Lake, P. B. Lindley, The mechanical fatigue limit for rubber. *J. Appl. Polym. Sci.* **9**, 1233–1251 (1965).
- S. Mzabi, D. Bergehan, S. Roux, F. Hild, C. Creton, A critical local energy release rate criterion for fatigue fracture of elastomers. *J. Polym. Sci. Part B Polym. Phys.* **49**, 1518–1524 (2011).
- C. Li, H. Yang, Z. Suo, J. Tang, Fatigue-Resistant elastomers. *J. Mech. Phys. Solids* **134**, 103751 (2020).
- J. Tang, J. Li, J. J. Vlassak, Z. Suo, Fatigue fracture of hydrogels. *Extrem. Mech. Lett.* **10**, 24–31 (2017).
- R. Bai, Q. Yang, J. Tang, X. P. Morelle, J. Vlassak, Z. Suo, Fatigue fracture of tough hydrogels. *Extrem. Mech. Lett.* **15**, 91–96 (2017).
- W. Zhang, X. Liu, J. Wang, J. Tang, J. Hu, T. Lu, Z. Suo, Fatigue of double-network hydrogels. *Eng. Fract. Mech.* **187**, 74–93 (2018).
- R. Bai, J. Yang, Z. Suo, Fatigue of hydrogels. *Eur. J. Mech. A/Solids* **74**, 337–370 (2019).
- J.-Y. Sun, X. Zhao, W. R. K. Illeperuma, O. Chaudhuri, K. H. Oh, D. J. Mooney, J. J. Vlassak, Z. Suo, Highly stretchable and tough hydrogels. *Nature* **489**, 133–136 (2012).
- P. Millereau, E. Ducrot, J. M. Clough, M. E. Wiseman, H. R. Brown, R. P. Sijbesma, C. Creton, Mechanics of elastomeric molecular composites. *Proc. Natl. Acad. Sci.* **115**, 9110–9115 (2018).
- Y. Tanaka, R. Kuwabara, Y.-H. Na, T. Kurokawa, J. P. Gong, Y. Osada, Determination of fracture energy of high strength double network hydrogels. *J. Phys. Chem. B* **109**, 11559–11562 (2005).
- E. Ducrot, Y. Chen, M. Bulters, R. P. Sijbesma, C. Creton, Toughening elastomers with sacrificial bonds and watching them break. *Science* **344**, 186–189 (2014).
- R. Göstl, R. P. Sijbesma,  $\pi$ -extended anthracenes as sensitive probes for mechanical stress. *Chem. Sci.* **7**, 370–375 (2016).
- M. Stratigaki, C. Baumann, L. C. A. van Breemen, J. P. A. Heuts, R. P. Sijbesma, R. Göstl, Fractography of poly(N-isopropylacrylamide) hydrogel networks crosslinked with mechanofluorophores using confocal laser scanning microscopy. *Polym. Chem.* **11**, 358–366 (2020).
- J. Slooman, V. Waltz, C. J. Yeh, C. Baumann, R. Göstl, J. Comtet, C. Creton, Quantifying rate- and temperature-dependent molecular damage in elastomer fracture. *Phys. Rev. X* **10**, 041045 (2020).
- J. P. Gong, Y. Katsuyama, T. Kurokawa, Y. Osada, Double-network hydrogels with extremely high mechanical strength. *Adv. Mater.* **15**, 1155–1158 (2003).
- R. E. Webber, C. Creton, H. R. Brown, J. P. Gong, Large strain hysteresis and Mullins effect of tough double-network hydrogels. *Macromolecules* **40**, 2919–2927 (2007).
- R. S. Rivlin, A. G. Thomas, in *Collected Papers of R.S. Rivlin* (Springer New York, New York, NY, 1997), vol. X, pp. 2615–2642; [http://link.springer.com/10.1007/978-1-4612-2416-7\\_180](http://link.springer.com/10.1007/978-1-4612-2416-7_180).
- R. Long, C.-Y. Hui, Fracture toughness of hydrogels: Measurement and interpretation. *Soft Matter* **12**, 8069–8086 (2016).
- H. Tsukeshiba, M. Huang, Y.-H. Na, T. Kurokawa, R. Kuwabara, Y. Tanaka, H. Furukawa, Y. Osada, J. P. Gong, Effect of polymer entanglement on the toughening of double network hydrogels. *J. Phys. Chem. B* **109**, 16304–16309 (2005).
- Y. N. Lenets, Near-threshold fatigue-crack growth: State of the problem and some anomalies. *Mater. Sci.* **30**, 301–315 (1995).
- G. J. Lake, A. G. Thomas, The strength of highly elastic materials. *Proc. R. Soc. A Math. Phys. Eng. Sci.* **300**, 108–119 (1967).
- A. Ahagon, A. N. Gent, Threshold fracture energies for elastomers. *J. Polym. Sci. Polym. Phys. Ed.* **13**, 1903–1911 (1975).
- A. N. Gent, R. H. Tobias, Threshold tear strength of elastomers. *J. Polym. Sci. Polym. Phys. Ed.* **20**, 2051–2058 (1982).
- J. G. Williams, A model of fatigue crack growth in polymers. *J. Mater. Sci.* **12**, 2525–2533 (1977).
- F. F. C. Dubach, W. G. Ellenbroek, C. Storm, How accurately do mechanophores report on bond scission in soft polymer materials? *J. Polym. Sci.* **59**, 1188–1199 (2021).
- S. Wang, S. Panyukov, M. Rubinstein, S. L. Craig, Quantitative adjustment to the molecular energy parameter in the Lake–Thomas theory of polymer fracture energy. *Macromolecules* **52**, 2772–2777 (2019).
- Y. Chen, C. J. Yeh, Y. Qi, R. Long, C. Creton, From force-responsive molecules to quantifying and mapping stresses in soft materials. *Sci. Adv.* **6**, eaaz5093 (2020).
- G. Bell, Models for the specific adhesion of cells to cells. *Science* **200**, 618–627 (1978).
- R. Merkel, P. Nassoy, A. Leung, K. Ritchie, E. Evans, Energy landscapes of receptor–ligand bonds explored with dynamic force spectroscopy. *Nature* **397**, 50–53 (1999).
- R. Long, C.-Y. Hui, J. P. Gong, E. Bouchbinder, The fracture of highly deformable soft materials: A tale of two length scales. *Annu. Rev. Condens. Matter Phys.* **12**, 71–94 (2021).
- Y. Chen, C. J. Yeh, Q. Guo, Y. Qi, R. Long, C. Creton, Fast reversible isomerization of merocyanine as a tool to quantify stress history in elastomers. *Chem. Sci.* **12**, 1693–1701 (2021).
- H. R. Brown, A molecular interpretation of the toughness of glassy polymers. *Macromolecules* **24**, 2752–2756 (1991).
- H. R. Brown, A model of the fracture of double network gels. *Macromolecules* **40**, 3815–3818 (2007).
- X. P. Morelle, G. E. Sanoja, S. Castagnet, C. Creton, 3D fluorescent mapping of invisible molecular damage after cavitation in hydrogen exposed elastomers. *Soft Matter* **17**, 4266–4274 (2021).
- A. Arora, T.-S. Lin, H. K. Beech, H. Mochigase, R. Wang, B. D. Olsen, Fracture of polymer networks containing topological defects. *Macromolecules* **53**, 7346–7355 (2020).
- S. Lin, X. Zhao, Fracture of polymer networks with diverse topological defects. *Phys. Rev. E* **102**, 052503 (2020).
- Z. Wang, C. Xiang, X. Yao, P. Le Floch, J. Mendez, Z. Suo, Stretchable materials of high toughness and low hysteresis. *Proc. Natl. Acad. Sci. U.S.A.* **116**, 5967–5972 (2019).
- J. Liu, C. Yang, T. Yin, Z. Wang, S. Qu, Z. Suo, Polyacrylamide hydrogels. II. Elastic dissipater. *J. Mech. Phys. Solids* **133**, 103737 (2019).
- S. Lin, X. Liu, J. Liu, H. Yuk, H.-C. Loh, G. A. Parada, C. Settens, J. Song, A. Masic, G. H. McKinley, X. Zhao, Anti-fatigue-fracture hydrogels. *Sci. Adv.* **5**, eaau8528 (2019).
- S. Lin, J. Liu, X. Liu, X. Zhao, Muscle-like fatigue-resistant hydrogels by mechanical training. *Proc. Natl. Acad. Sci. U.S.A.* **116**, 10244–10249 (2019).

46. M. Rubinstein, S. Panyukov, Elasticity of polymer networks. *Macromolecules* **35**, 6670–6686 (2002).
47. L. Léger, C. Creton, Adhesion mechanisms at soft polymer interfaces. *Philos. Trans. R. Soc. A Math. Phys. Eng. Sci.* **366**, 1425–1442 (2008).

**Acknowledgments:** SEM images were collected with support from Guillaume Votte.

**Funding:** This work was supported by the European Research Council (ERC) under the European Union's Horizon 2020 Research and Innovation Program (grant agreement no. 695351, CHEMECH). X.P.M. was financially supported by the WBI world excellence postdoctoral fellowship. **Author contributions:** Research was designed by G.E.S., X.P.M., and C.C. Synthesis was conducted by G.E.S. Specimens were mechanically tested by G.E.S. and X.P.M. Damage was visualized and quantified by G.E.S., J.C., and C.J.Y. The manuscript was written by G.E.S. and was critically revised by all authors. All authors have given final approval to the final

version of the manuscript. **Competing interests:** The authors declare that they have no competing interests. **Data and materials availability:** All data needed to evaluate the conclusions in the paper are present in the paper and/or the Supplementary Materials, as well as in the Texas Data Repository.

Submitted 5 February 2021

Accepted 20 August 2021

Published 13 October 2021

10.1126/sciadv.abg9410

**Citation:** G. E. Sanoja, X. P. Morelle, J. Comtet, C. J. Yeh, M. Ciccotti, C. Creton, Why is mechanical fatigue different from toughness in elastomers? The role of damage by polymer chain scission. *Sci. Adv.* **7**, eabg9410 (2021).

## Why is mechanical fatigue different from toughness in elastomers? The role of damage by polymer chain scission

Gabriel E. SanojaXavier P. MorelleJean ComtetC. Joshua YehMatteo CiccottiCostantino Creton

*Sci. Adv.*, 7 (42), eabg9410. • DOI: 10.1126/sciadv.abg9410

### View the article online

<https://www.science.org/doi/10.1126/sciadv.abg9410>

### Permissions

<https://www.science.org/help/reprints-and-permissions>

Use of think article is subject to the [Terms of service](#)

---

*Science Advances* (ISSN ) is published by the American Association for the Advancement of Science. 1200 New York Avenue NW, Washington, DC 20005. The title *Science Advances* is a registered trademark of AAAS. Copyright © 2021 The Authors, some rights reserved; exclusive licensee American Association for the Advancement of Science. No claim to original U.S. Government Works. Distributed under a Creative Commons Attribution NonCommercial License 4.0 (CC BY-NC).